Entropic selectivity of binary mixtures in cylindrical pores

A. González,[1] J. A. White,[1,a)] F. L. Román,[2] and S. Velasco[1]
[1]*Departamento de Física Aplicada, Universidad de Salamanca, E-37008 Salamanca, Spain*
[2]*Escuela Politécnica Superior de Zamora, Universidad de Salamanca, E-49022 Zamora, Spain*

(Received 1 July 2011; accepted 6 September 2011; published online 21 October 2011)

We show that a simple model consisting of a binary hard-sphere mixture in a narrow cylindrical pore can lead to strong size selectivity by considering a situation where each species of the mixture *sees* a different radius of the cylinder. Two mechanisms are proposed to explain the observed results depending on the radius of the cylinder: for large radii the selectivity is driven by an enhancement of the depletion forces at the cylinder walls whereas for the narrowest cylinders excluded-volume effects lead to a shift of the effective chemical potential of the particles in the pore. © *2011 American Institute of Physics*. [doi:10.1063/1.3643117]

I. INTRODUCTION

A few years ago, Goulding and co-workers[1] examined the size selectivity of narrow pores within the framework of density functional theory (DFT). They showed that purely steric (excluded volume) effects can lead to strong size selectivity in a ternary hard-sphere (HS) mixture in an infinite cylindrical pore with a radius R_c of dimensions comparable to the diameters σ_i's of the particles. Later, Roth and Gillespie[2] considered different entropic mechanisms that can lead to size selectivity both in ternary and binary HS mixtures. More recently, Roth *et al.*[3] investigated the effect of external potentials on the selectivity of particles both from a static and dynamical point of view.

These simple models have direct application to the physics of biological ion channels[4] where selectivity arises from the balance of electrostatics and steric effects.[5] We note, however, that neglecting electrostatic interactions did not alter significantly the selectivity in the model of Goulding *et al.*[1] and therefore, investigating new excluded-volume mechanisms for particle selectivity can provide further insight in the engineering of ion channels.[6]

This work is focused in this aspect, and therefore we look for purely entropic situations that can give rise to strong selectivity. In particular, in the present work we will show that a simple model consisting of a binary HS mixture in a hard cylindrical nanopore can lead to strong size selectivity by considering different radii $R_{c,i}$ of the cylinder for each species (see Fig. 1). This implies that the external potential depends on the species i, namely,

$$V_{\text{ext},i}(r) = \begin{cases} 0, & r < R_{c,i} - \sigma_i/2 \\ \infty, & r > R_{c,i} - \sigma_i/2 \end{cases}, \tag{1}$$

where r is the distance from the center of the hard-sphere to the axis of the cylinder and σ_i is the diameter of species i.

We would like to note that the external potential (1) could be experimentally realized by using an appropriate stationary extended pattern of light (optical landscape). This optical landscape can show a strong dependence on the size, the shape or the refractive index of dielectric microscopic particles (see Ref. 7, and references therein).

Following Goulding *et al.*[1] we define the absorbance of species i to be the ratio $\xi_i = \bar{\eta}_i/\eta_{b,i}$ where $\bar{\eta}_i$ is the average packing fraction of species i within the pore, i.e., $\bar{\eta}_i = v_i\langle N_i\rangle/V_i$, where $v_i \equiv \pi\sigma_i^3/6$ is the volume of one particle and V_i is the total volume of a cylinder of radius $R_{c,i}$ and length L containing an average number of particles $\langle N_i\rangle$. Recall that we work in the grand-canonical ensemble by assuming that the inhomogeneous system can exchange particles with a reservoir characterized by the bulk packing fractions $\eta_{b,i}$'s. The selectivity of species 1 over species 2 is defined as $\xi_{12} = \xi_1/\xi_2$. With this definition, species 1 is selected preferentially over species 2 if $\xi_{12} > 1$.

The analysis of the model will be made by means of DFT calculations which are computationally much less demanding than Monte Carlo simulations. Among the different DFT prescriptions we choose the fundamental measures theory (FMT) which has become a standard nowadays both because of its accuracy and its ease of implementation.

II. DENSITY FUNCTIONAL THEORY

Since the original formulation of the FMT (Ref. 8) several versions of the theory have been published for hard spheres[9–16] (for recent reviews see Refs. 17 and 18). In this work we shall consider very narrow cylindrical pores in which quasi one-dimensional confinement may arise. For these highly inhomogeneous situations the choice of a particular version of the FMT might be critical[19] and therefore, prior to the calculation of the selectivity in the pore, we will analyze the performance of some FMT versions in order to choose the most appropriate for the present problem.

The FMT excess (over ideal) contribution $\mathcal{F}_{ex}[\rho]$ to the free-energy functional is assumed to take the form

$$\beta\mathcal{F}_{ex}[\rho] = \beta\mathcal{F}[\rho] - \beta\mathcal{F}_{id}[\rho] = \int d\mathbf{r}\, \Phi[\rho], \tag{2}$$

where $\rho = \{\rho_i(\mathbf{r})\}$ indicates the set of densities of the inhomogeneous mixture, being $\beta = 1/k_BT$ the inverse temperature.

a)Also at IUFFyM, Universidad de Salamanca, Spain. Electronic mail: white@usal.es.

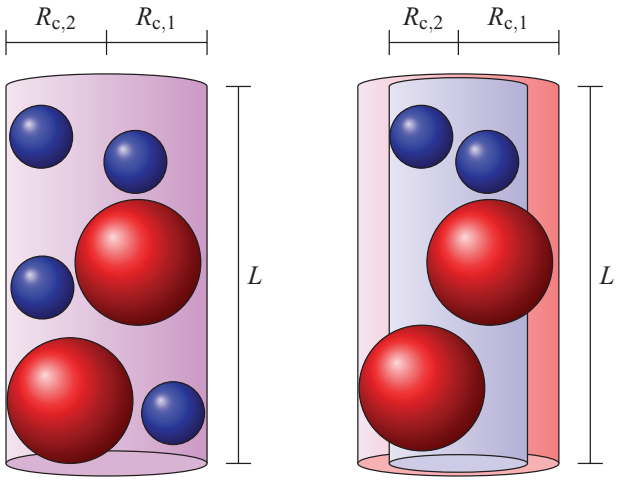

(a) Equal radii (b) Different radii

FIG. 1. Hard-sphere binary mixture in a hard cylindrical nanopore.

In this equation $\beta^{-1}\Phi$ is the excess free-energy density and quite generally it can be expressed as a sum of three contributions,

$$\Phi = \Phi_1 + \Phi_2 + \Phi_3\,. \tag{3}$$

In the original formulation of the FMT (Ref. 8) for a HS mixture these contributions take the form[14]

$$\Phi_1 = -\sum_i n_i(\mathbf{r})\log[1-\eta(\mathbf{r})], \tag{4}$$

$$\Phi_2 = 2\pi\sum_{i,j} R_i R_j (R_i + R_j)\frac{(n_i(\mathbf{r})n_j(\mathbf{r}) - \mathbf{v}_i(\mathbf{r})\cdot\mathbf{v}_j(\mathbf{r}))}{1-\eta(\mathbf{r})}, \tag{5}$$

$$\Phi_3 = 8\pi^2\sum_{i,j,k} R_i^2 R_j^2 R_k^2 n_i(\mathbf{r})\frac{\frac{1}{3}n_j(\mathbf{r})n_k(\mathbf{r}) - \mathbf{v}_j(\mathbf{r})\cdot\mathbf{v}_k(\mathbf{r})}{(1-\eta(\mathbf{r}))^2}, \tag{6}$$

where $R_i = \sigma_i/2$ is the radius of species i. $\eta(\mathbf{r})$ and the $n_i(\mathbf{r})$'s are scalar weighted densities, and the $\mathbf{v}_i(\mathbf{r})$'s are vector weighted densities. These weighted densities are defined by

$$\eta(\mathbf{r}) = \sum_i \int \rho_i(\mathbf{r}')\theta(R_i - |\mathbf{r}-\mathbf{r}'|)\,d\mathbf{r}', \tag{7}$$

$$n_i(\mathbf{r}) = \frac{1}{4\pi R_i^2}\int \rho_i(\mathbf{r}')\delta(R_i - |\mathbf{r}-\mathbf{r}'|)\,d\mathbf{r}', \tag{8}$$

$$\mathbf{v}_i(\mathbf{r}) = \frac{1}{4\pi R_i^2}\int \rho_i(\mathbf{r}')\delta(R_i - |\mathbf{r}-\mathbf{r}'|)\widehat{(\mathbf{r}-\mathbf{r}')}\,d\mathbf{r}', \tag{9}$$

where $\widehat{\mathbf{r}} \equiv \mathbf{r}/r$ is a unit vector.

The main issue of the original version of the FMT (Ref. 8) is its failure to yield the correct dimensional crossover to zero and one dimensions which implies a lack of accuracy in describing highly inhomogeneous situations where the fluid is confined to quasi zero-dimensional (0D) cavities or quasi-1D nanopores.[19] Since in this work we consider very narrow cylindrical pores where quasi-1D situations may arise, in addition to the original FMT prescription[8] we shall consider the tensorial version of the FMT developed by Tarazona[12] which has been shown to describe accurately these extreme situations for the one-component fluid.[19] Although Tarazona's tensorial FMT was initially formulated for the one-component fluid, it was subsequently extended to HS mixtures.[13,14] In the extension to mixtures developed by Cuesta *et al.*[14] the first two terms of Eq. (3) are still valid while the third term reads

$$\Phi_3 = 12\pi^2\sum_{i,j,k} R_i^2 R_j^2 R_k^2 \frac{\phi_{ijk}(\mathbf{r})}{(1-\eta(\mathbf{r}))^2}, \tag{10}$$

where

$$\phi_{ijk} = \mathbf{v}_i\cdot T_j\cdot\mathbf{v}_k - n_j\mathbf{v}_i\cdot\mathbf{v}_k - \mathrm{tr}(T_iT_jT_k) + n_j\mathrm{tr}(T_iT_k). \tag{11}$$

In this equation tr() indicates the trace operator, and T_i is a rank-2 tensor weighted density defined as

$$T_i^{(a,b)}(\mathbf{r}) = \frac{1}{4\pi R_i^2}\int \rho_i(\mathbf{r}')\delta(R_i - |\mathbf{r}-\mathbf{r}'|) \tag{12}$$

$$\times(\widehat{\mathbf{r}-\mathbf{r}'})_a(\widehat{\mathbf{r}-\mathbf{r}'})_b\,d\mathbf{r}', \tag{13}$$

where $a, b = x, y, z$ are Cartesian coordinates.

Cuesta *et al.*[14] showed that the above extension to mixtures fails to yield the exact crossover from three to one dimensions and then proposed another tensorial FMT with the correct 1D limit for HS mixtures but presenting additional complexity due to the use of rank-3 tensor measures (see Ref. 14 for details).

The results of Rosenfeld's original FMT and of Tarazona's tensorial FMT have been obtained in the usual way by solving the coupled Euler-Lagrange equations for the density profiles $\rho_i(r)$ of the species i in the cylindrical pore by means of an iterative procedure and taking profit of the symmetry of the problem.[19] The solution of the correction to the tensorial FMT is more difficult to handle by this method due to the complexity of the free energy functional involving tensorial weighted densities of rank 3.[14] In this case we have considered a different approach consisting in a direct minimization of the free energy of the system by means of a slower but easier to implement simulated-annealing method: random changes of the density profile at random positions are performed, so that the changes leading to a smaller value of the free energy are always accepted, while the changes that lead to a higher value of the free energy are accepted with a probability P that depend on a synthetic temperature $\hat{T}$. The jumps to higher free energy solutions prevent the system to get stuck on local minima. Along the simulation $\hat{T}$ is slowly decreased towards 0 so that $P(\hat{T}) \to 0$.

III. RESULTS AND DISCUSSION

To keep things simple, in this work we have restricted ourselves to a binary HS mixture where species 1 consists of big particles of diameter σ_1 and species 2 consists of small particles of diameter $\sigma_2 = \sigma_1/2$ (other similar ratios yield

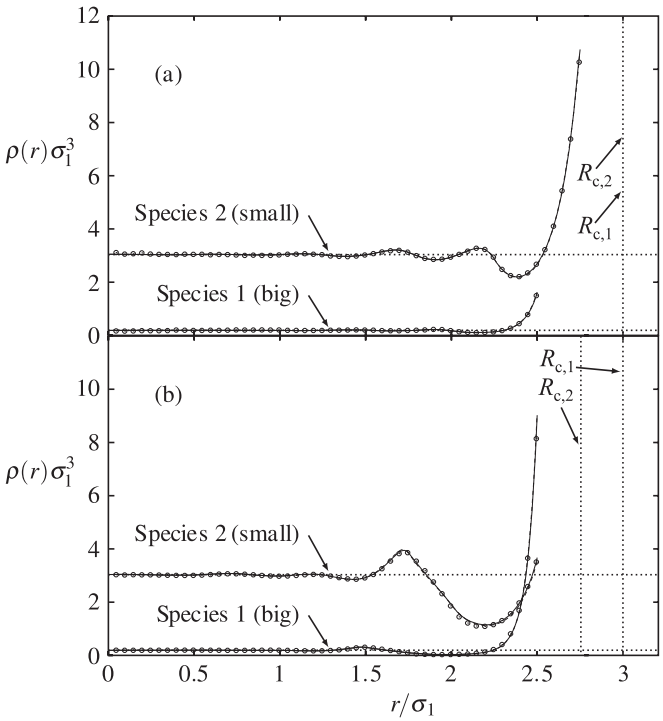

FIG. 2. Density profiles for a HS mixture in a cylindrical pore. $\eta_{b,1} \cong 0.1$ and $\eta_{b,2} \cong 0.2$. (a) $R_{c,1} = R_{c,2} = 3\sigma_1$ and (b) $R_{c,1} = 3\sigma_1$ and $R_{c,2} = 2.75\sigma_1$. The solid and dashed lines are the results of the tensorial FMT and the original FMT, respectively. Symbols: CEMC simulations. The horizontal dotted lines indicate the bulk densities and the vertical dotted lines indicate the position of the radius of the cylinder for each species. $\sigma_2 = \sigma_1/2$.

qualitatively similar results). In Fig. 2(a) we present our results for the density profiles $\rho_i(r)$ in a cylindrical pore with equal radius for each species $R_{c,1} = R_{c,2} = 3\sigma_1$ (this means that the radial distance available to the centers of the particles depends on the species). For the present situation in which the radius of the pore is not very small the results of the tensorial FMT and of its correction are almost indistinguishable and the same happens for the original Rosenfeld's FMT. In order to determine the accuracy of the FMT-DFT calculations we also compare with the results of our Monte Carlo simulations. In this particular case the usual grand canonical ensemble Monte Carlo (GCEMC) simulations[20] of the HS fluid in a cylindrical pore[21] present important equilibration problems and we have opted for canonical ensemble Monte Carlo (CEMC) simulations which, given the large number of particles involved ($N_1 = 24$, $N_2 = 400$ for a cylinder of length $L = 5\sigma_1$) should yield the same results than a GCEMC simulation for a system with equal mean numbers of particles.[21,22] The FMT calculations have been made so that they also yield the same mean numbers of particles; this implies a reservoir with bulk packing fractions $\eta_{b,1} = 0.099558 \cong 0.1$ and $\eta_{b,2} = 0.19881 \cong 0.2$ for the tensorial FMT. Very similar results are obtained for the other DFT's. We would like to note that the density profiles at the center of the cylinder become almost constant, reaching the homogeneous limit, with the same densities ($\rho_{b,1} = 6\eta_{b,1}/\pi\sigma_1^3 = 0.190142\sigma_1^{-3}$ and $\rho_{b,2} = 6\eta_{b,2}/\pi\sigma_2^3 = 3.0376\sigma_1^{-3}$).

Apart from showing the excellent performance of all FMT-DFT calculations, Fig. 2(a) does not deserve any additional comments: it presents a perfectly normal situation for a HS mixture in a pore. Things are very different in Fig. 2(b) where the radius of the cylinder for each species is different: $R_{c,1} = 3\sigma_1$ and $R_{c,2} = 2.75\sigma_1$ (note that, for this particular case, this implies in turn equal radial distance available to the centers of the particles, independent on the species). In this case with similar bulk packing fractions ($\eta_{b,1} = 0.100828$ and $\eta_{b,2} = 0.198384$) the mean number of adsorbed particles for species 1 raises from $\langle N_1 \rangle = 24$ to 54 in spite of having the same cylinder radius than in the previous case. Of course, the mean number of adsorbed particles for species 2 lowers from $\langle N_2 \rangle = 400$ to 250 due to the smaller cylinder radius and the larger density of species 1 at contact. Again we note that both species reach the expected homogeneous limit at the center of the cavity. The reason for this increase in $\langle N_1 \rangle$ is clearly due to an enhancement of the depletion potential acting over the big particles (species 1) at the pore walls: the absence of small particles (species 2) between $R_{c,2}$ and $R_{c,1}$ implies that this volume can only be optimally occupied if many big particles are located near the cylinder walls, as it is shown in Fig. 2(b) where the density of species 1 at contact is about five times larger than in Fig. 2(a). Very small differences can be observed between the results of the tensorial FMT and the original Rosenfeld's FMT with very good agreement with simulation although the tensorial theory seems to fare slightly better. The correction to the tensorial theory (not shown) yields results that are indistinguishable from those of the uncorrected tensorial FMT.

In Fig. 3(a) we consider a very narrow pore with equal radius for each species $R_{c,1} = R_{c,2} = 0.8\sigma_1$ in contact with a reservoir characterized by the bulk packing fractions $\eta_{b,1} = 0.05$, $\eta_{b,2} = 0.15$. Although the packing in the reservoir is lower than that of Fig. 2 the much smaller cylinder radius leads to a very inhomogeneous quasi-1D situation. In spite of

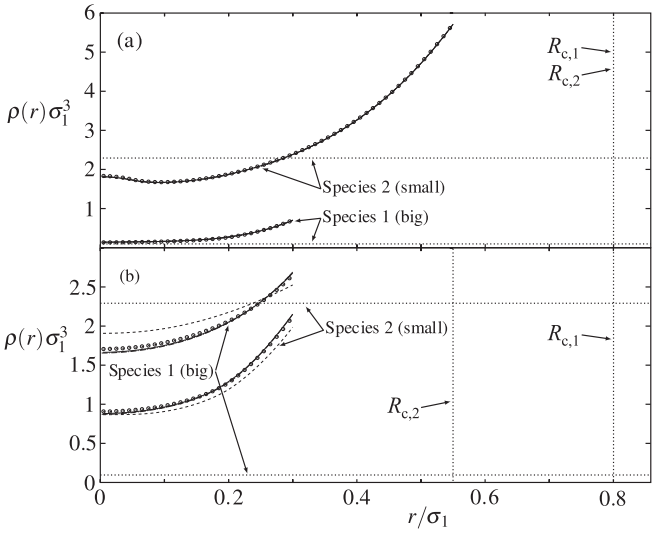

FIG. 3. Density profiles for a HS mixture in a narrow cylindrical pore. $\eta_{b,1} = 0.05$ and $\eta_{b,2} = 0.15$. (a) $R_{c,1} = R_{c,2} = 0.8\sigma_1$ and (b) $R_{c,1} = 0.8\sigma_1$ and $R_{c,2} = 0.55\sigma_1$. The solid, dot-dashed, and dashed lines are the results of the tensorial FMT, its correction, and the original FMT, respectively. Symbols: GCEMC simulations. The horizontal dotted lines indicate the bulk densities and the vertical dotted lines indicate the position of the radius of the cylinder for each species. $\sigma_2 = \sigma_1/2$.

this, we obtain excellent agreement between all of the considered FMT prescriptions and GCEMC simulation which, for this particular case, yields reliable results. We note that species 1 approximately reaches the homogeneous limit in the center of the cylinder whereas species 2 does not. In this case we do not observe any noticeable increase in the absorbance of the considered species. However, in Fig. 3(b), with different radii for each species ($R_{c,1} = 0.8\,\sigma_1$ and $R_{c,2} = 0.55\,\sigma_1$), the situation becomes very different. In this case we observe that the original Rosenfeld's FMT no longer yields accurate results, with a significant deviation from GCEMC data for both species. The tensorial FMT and its correction yield almost the same results with very small differences with simulation, slightly overestimating the density at contact with the pore wall and underestimating it at the center of the pore, specially for species 1. We note that the tensorial FMT fares a bit better than its correction. The results shown in this figure have led us to consider the tensorial FMT in the forthcoming calculations since its computational complexity is comparable to that of the original Rosenfeld theory and, as expected, yields much better results in extremely confined quasi-1D situations like the ones considered in this paper.

The most remarkable feature of Fig. 3(b) is the fact that the average density for the big particles inside the pore is much larger than the bulk density whereas the opposite happens for the small particles. This implies a very large absorbance for species 1 and a small absorbance for the species 2 which leads to a large selectivity $\xi_{12} \cong 17$ of species 1 over species 2 (note that the volume occupied by one big particle is 8 times that of one small particle). Certainly, this somehow unexpected result is due to the different pore radius *seen* by each species but in this case it cannot straightforwardly be ascribed to an enhancement in the wall-particle depletion potential like in the case presented in Fig. 2(b). Rather, we explain this behavior by observing that the species that *sees* a smaller cylinder radius is subjected to an effective repulsive potential due to the particles of the other species occupying the extra volume and this leads to a selective absorption of the latter. A similar finding was made by Roth and Gillespie[2]

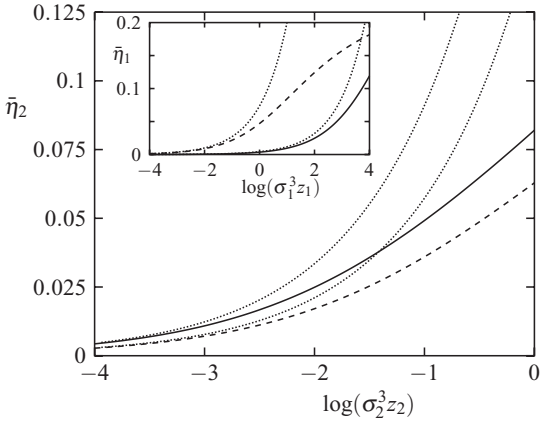

FIG. 4. Average packing fraction in the pore $\bar{\eta}_i$ vs. the chemical potential $\log \sigma_i^3 z_i = \beta\mu_i - 3\log\Lambda_i/\sigma_i$. (Solid lines) $R_{c,1} = 0.55\,\sigma_1$ and $R_{c,2} = 0.8\,\sigma_1$. (Dashed lines) $R_{c,1} = 0.8\,\sigma_1$ and $R_{c,2} = 0.55\,\sigma_1$. (Dotted lines) results of Eq. (14). $\sigma_2 = \sigma_1/2$. (Main panel) species 2; $\log \sigma_1^3 z_1 = -4$. (Inset) species 1; $\log \sigma_2^3 z_2 = -4$.

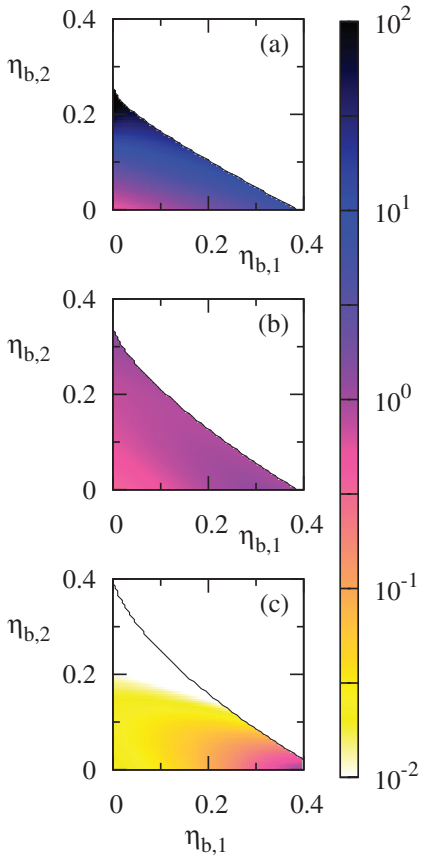

FIG. 5. Density map of the selectivity $\xi_{12} = \xi_1/\xi_2$ vs. the bulk packing fractions of the mixture. (a) $R_{c,1} = 0.8\sigma_1$, $R_{c,2} = 0.55\sigma_1$. (b) $R_{c,1} = 0.8\sigma_1$, $R_{c,2} = 0.8\sigma_1$. (c) $R_{c,1} = 0.55\sigma_1$, $R_{c,2} = 0.8\sigma_1$. The lines show the convergence limit of the DFT calculations. $\sigma_2 = \sigma_1/2$.

by explicitly including such effective potential in their model of ion channels. The effective repulsive potential can be interpreted as a *shift* in the chemical potential of the species in the pore so that their average packing fractions are increased or decreased with respect to a system with equal pore radii. This shift is shown in Fig. 4 where in addition to the DFT results we also plot (dotted lines) the following upper bound for the average packing fraction

$$\bar{\eta}_i \leq \frac{\pi \sigma_i^3 z_i}{6}\left(\frac{R_{c,i} - \sigma_i/2}{R_{c,i}}\right)^2, \tag{14}$$

which should be valid at low packings and was obtained from an upper bound to the absorbance obtained by Goulding *et al.*[1] In Eq. (14) z_i is the affinity of species i, defined as

$$z_i = \Lambda_i^{-3} e^{\beta\mu_i}, \tag{15}$$

where μ_i and Λ_i are, respectively, the chemical potential and the thermal de Broglie wavelength of species i. Multiplying both sides of Eq. (15) by σ_i^3 and taking logarithms one obtains

$$\log \sigma_i^3 z_i = \beta\mu_i - 3\log\Lambda_i/\sigma_i\,. \tag{16}$$

Thus the logarithm of the affinity is essentially the chemical potential. For convenience, this is the quantity used in the abscissae of Fig. 4. From the upper bound of Eq. (14) it becomes clear that changing the radius $R_{c,i}$ leads to a shift in μ_i: keeping constant $\bar{\eta}_i$ implies that a decrease in $(R_{c,i} - \sigma_i/2)^2/R_{c,i}^2$

should lead to an increase in z_i (and thus in μ_i) and vice versa, these changes being larger for $R_{c,i}$ close to $\sigma_i/2$. In Fig. 4 we present results for a pore with $R_{c,1} = 0.55\,\sigma_1$ and $R_{c,2} = 0.8\,\sigma_1$ (solid lines) and for a pore with $R_{c,1} = 0.8\,\sigma_1$ and $R_{c,2} = 0.55\,\sigma_1$ (dashed lines). These results show that the chemical potential of the species that *see* the smaller cylinder radius is shifted towards the right, in accordance with Eq. (14). For clarity, the results for a pore with $R_{c,1} = 0.8\,\sigma_1$ and $R_{c,2} = 0.8\,\sigma_1$ are not shown, but as expected, they are very close to the dashed line in the inset ($R_{c,1} = 0.8$) and indistinguishable from the solid line in the main panel ($R_{c,2} = 0.8$).

Finally, in Fig. 5 we present our tensorial FMT results for the selectivity ξ_{12} of species 1 over species 2 ($\sigma_2 = \sigma_1/2$). In Fig. 5(a) we consider a situation where $R_{c,1} = 0.8\sigma_1$ and $R_{c,2} = 0.55\sigma_1$ and we observe how the big particles (species 1) are preferentially absorbed over the smaller ones. The opposite happens in Fig. 5(c) where the small particles are selected over the large ones. In Fig. 5(b) we see that a situation with equal radii lead to similar absorbances for both species. Clearly, this behavior is related to the fact that the species with more free-volume available is preferentially selected by the pore, as commented in Fig. 4.

ACKNOWLEDGMENTS

J.A.W. thanks J. A. Cuesta, Y. Martínez-Ratón, and P. Tarazona for discussions at the initial stages of this work. We are grateful for financial support from the Ministerio de Ciencia e Innovación of Spain (Grant No. FIS2009-07557/FEDER).

[1] D. Goulding, J.-P. Hansen, and S. Melchionna, Phys. Rev. Lett. **85**, 1132 (2000); D. Goulding, S. Melchionna, and J.-P. Hansen, Phys. Chem. Chem. Phys. **3**, 1644 (2001).
[2] R. Roth and D. Gillespie, Phys. Rev. Lett. **95**, 247801 (2005).
[3] R. Roth, M. Rauscher, and A. Archer, Phys. Rev. E **80**, 021409 (2009).
[4] B. Hille, *Ion Channels of Excitable Membranes* (Sinauer Associates, Sunderland, MA, 2001).
[5] D. Boda, W. Nonner, M. Valiskó, D. Henderson, B. Eisenberg, and D. Gillespie, Biophys. J. **93**, 1960 (2007).
[6] B. Eisenberg, Proc. Natl. Acad. Sci. U.S.A. **105**, 6211 (2008).
[7] G. Milne, K. Dholakia, D. McGloin, K. Volke-Sepulveda, and P. Zemánek, Opt. Express **15**, 13972 (2007).
[8] Y. Rosenfeld, Phys. Rev. Lett. **63**, 980 (1989).
[9] E. Kierlik and M. L. Rosinberg, Phys. Rev. A **42**, 3382 (1990).
[10] Y. Rosenfeld, M. Schmidt, H. Löwen, and P. Tarazona, J. Phys.: Condens. Matter **8**, L577 (1996); Phys. Rev. E **55**, 4245 (1997).
[11] A. González, J. A. White, and R. Evans, J. Phys.: Condens. Matter **9**, 2375 (1997); A. González and J. A. White, Physica A **296**, 347 (2001).
[12] P. Tarazona, Phys. Rev. Lett. **84**, 694 (2000); Physica A **306**, 243 (2002).
[13] M. Schmidt, H. Löwen, J. Brader, and R. Evans, Phys. Rev. Lett. **85**, 1934 (2000).
[14] J. A. Cuesta, Y. Martínez-Ratón, and P. Tarazona, J. Phys.: Condens. Matter **14**, 11965 (2002).
[15] R. Roth, R. Evans, A. Lang, and G. Kahl, J. Phys.: Condens. Matter **14**, 12063 (2002).
[16] Y.-X. Yu and J. Wu, J. Chem. Phys. **117**, 10156 (2002).
[17] P. Tarazona, J. A. Cuesta, and Y. Martinez-Ratón, in *Theory and Simulation of Hard-Sphere Fluids and Related Systems*, Lecture Notes in Physics Vol. 753, edited by A. Mulero (Springer-Verlag, Berlin, 2008), pp. 247–341.
[18] R. Roth, J. Phys.: Condens. Matter **22**, 063102 (2010).
[19] A. González, J. A. White, F. L. Román, and S. Velasco, J. Chem. Phys. **125**, 064703 (2006).
[20] D. Frenkel and B. Smit, *Understanding Molecular Simulation* (Academic, London, 1996).
[21] F. L. Román, J. A. White, A. González, and S. Velasco, J. Chem. Phys. **124**, 154708 (2006).
[22] A. González, J. A. White, F. L. Román, S. Velasco, and R. Evans, Phys. Rev. Lett. **79**, 2466 (1997); A. González, J. A. White, F. L. Román, and R. Evans, J. Chem. Phys. **109**, 3637 (1998).